The 9th International Symposium on Transport Phenomena and
Dynamics of Rotating Machinery
Honolulu, Hawaii, February 10-14, 2002

TWO- AND THREE DIMENSIONAL NUMERICAL EXPERIMENTS REPRESENTING TWO LIMITING CASES OF AN IN-LINE PAIR OF FINGER SEAL COMPONENTS.

M.J. Braun
Department of Mechanical Engineering
University of Akron, Akron, OH 44325, USA
(mjbraun@uakron.edu)

V.V. Kudriavtsev
CFD Canada
Toronto, Ontario, M3A 3A3, Canada
(vvk@cfdcanada.com)

B.M. Steinetz
NASA Glenn Research Center
Cleveland, OH 44135

M.P. Proctor
NASA Glenn Research Center
Cleveland, OH 44135

ABSTRACT

The work presented here concerns the numerical development and simulation of the flow, pressure patterns and motion of a pair of fingers arranged behind each other and axially aligned in-line. The fingers represent the basic elemental component of a Finger Seal (FS) and form a tight seal around the rotor. Yet their flexibility allows compliance with rotor motion and in a passive-adaptive mode complies also with the hydrodynamic forces induced by the flowing fluid. While the paper does not treat the actual staggered configuration of a finger seal, the in-line arrangement represents a first step towards that final goal. The numerical 2-D (axial-radial) and 3-D results presented herein were obtained using a commercial package (CFD-ACE+). Both models use an integrated numerical approach, which couples the hydrodynamic fluid model (Navier-Stokes based) to the solid mechanics code that models the compliance of the fingers.

INTRODUCTION

For small diameter turbines (with short blades), wear of the blade tip is particularly troublesome since it generates a much larger percentage of leakage flow when compared to larger diameter turbines with a similar wear. The basic causes for clearance increase reside with the radial displacements of the rotor, which in time, creates clearances that are generally larger than the ones desired for efficient operation. These displacements can be caused by: (a) differential tandem thermal response of the case and the rotor caused by operational transients, (b) ovalization due to non-axisymmetric temperatures and/or loads, (c) centrifugal and gyroscopic loads and (d) thrust, maneuver or air turbulence loads. The real bottom line of the effect of seal leakages can be seen in the change in the SFC, engine effectiveness, and overhaul times. The leakage causes enumerated above are not necessarily specific to the turbine, but they also apply to the high (HPC) and low (LPC) pressure compressors, even though the thermal environment is generally less hostile. According to Ludwig (1978), the SFC can increase (due to leakage) by as much as 0.51% for the HPC, 0.58% for HPT and 0.69% for LPT. The compliant shroud/seal (whether outfitted with brush or finger seals) appears to be an ideal candidate for the role of passive-adaptive mitigation of this type of leakages. It will provide principally a compliant buffer for the HPT blades and due to its compliance will keep, over time, the operating clearances significantly smaller than the presently rigid shrouds. It should be noted that the technology of shaft compliant seals has been revolutionized about 15 years ago, when brush seals were proposed to replace the labyrinth seals at many locations along the compressor's and turbine's shafts. Today brush seals are in operation as shaft seals in Rolls-Royce, Pratt and Whitney and GE jet engines.

Brief Review of the State of the Art of Compliant Seals

Brush Seals (Figure 1a). Sealing at the brush seal/shaft interface is ensured by tight packing of the bristles and interference tolerance fit between the seal inner diameter and shaft outer diameter. Leakage occurs both at the brush/rotor interface and through the brush's bristle pack. It is now universally recognized that this embodiment is much more effective than the labyrinth seal and its deterioration is much delayed. There has been a considerable amount of experimental work that advanced the state of the art of these types of seals and we shall mention a few seminal contributions here (Ferguson [1988], Chupp et al. [1991], Proctor et al. [1996], Atkinson and Bristol [1992], Hendricks et al. [1992], Forry [1993]). During the same period, an effort was also afoot to validate numerical simulations through comparisons to the available experimental data. Thus, early on, Braun et al. [1990] and Hendricks et al. [1991], offered bulk flow model for flow through the body of a brush, based on analytical and experimental developments concerning flow in porous media. The analytical results, when compared with experimental data showed relatively good coincidence. The same year, Mullen et al. [1990]

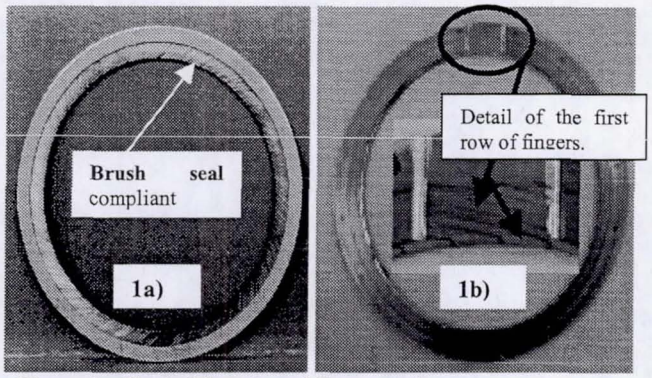

Figure 1. Typical brush and finger seals

presented numerical results based on a finite element model which simulated a flow field of 6x6 uniformly spaced bristle matrix. The maximum differential between the experimental and numerical results was observed at low flows, and was approximately 30%. Chupp and Holle [1991,1994] also offered alternate bulk flow models for leakage through a randomly distributed bristle bed.

Finger Seals (FS) (Figure 1b). These types of seals also represent a compliant seal configuration, Figure 2. There are earlier versions of the finger seal pioneered by Heydrich (1991), Mackay et al. (1991, 1991a), and Johnson et al. (1992). What differentiates FS and makes them preferable to the brush seals is their potential hydrodynamic lifting capabilities, and thus their non-contacting nature. The fingers' compliance allows both axial and radial adjustment to rotor excursions without damage to the integrity of the seal. Their potential lifting capability eliminates the wear factor, thus increasing considerably their life span relative to that of rigid seals. The fundamental geometry of a FS can be studied from Figures 1b and 2. The shape of the finger (stick+ pad) is etched

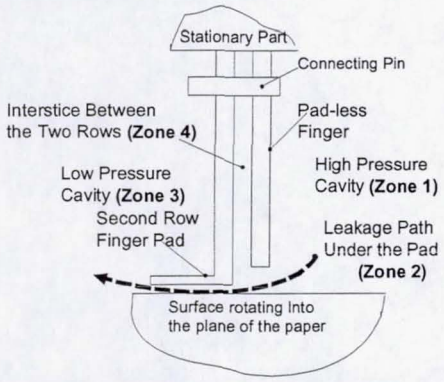

Figure 2. Finger seal two row configuration with finger pad on the high pressure side. Longitudinal cross section

chemically in the material by a photo process that allows the cutting of the thin interstices separating the individual fingers.

The stick ends with an enlarged formation that has a geometry similar to the pad shown in Figure 2. The root of the stick joins the annulus shown in Figure 1b from which the whole finger seal was cut. This configuration allows the finger to move freely like a cantilever beam in its space and thus exhibit compliance to the external forces acting on it. To form a full seal, two or more annular laminates are assembled axially in a staggered arrangement such that fingers from the upstream laminates cover the interstices between the fingers of the downstream laminates, Figure 1b. In general the width of the seal is such that in a turbine blade tip application it covers the entire axial width of the turbine blade while as shaft seals the width is chosen with lesser restrictions. In the latter embodiment the shaft seals have already been successfully tested as interstage and buffer seals at NASA Glenn Research Center. A report by Hendricks et al. (1994), reviews four compliant seal concepts, including FS that have the potential to be non-contacting seals. The authors provide a comparative table of experimental results that show contacting finger seal performance to be better in terms of leakage than both the labyrinth and brush seals. They also offer a bulk model analysis similar to the one performed by Braun and Hendricks (1990), Hendricks et al. (1991) for the brush seal. Steinetz et al. (1998) also mention the finger seal as potential film riding non-contacting candidate for both shaft and blade tip seals. Finally Arora et al. (1999) present a detailed evaluation experiment for a low hysteresis finger seal, find that the hysteresis and endurance performance were encouraging and that typical leakage is 20 to 70% less than that of a four knife labyrinth seal. The seal was operated up to speeds of 945 ft/sec (288m/s) and 80 psi (552 kPa) pressure differential.

SCOPE OF WORK

Just like the brush seals, the finger seals are mounted on the rotor with a certain interference fit. Finger seals exhibit two advantages over brush seals: (a) the manufacturing process costs are much lower when compared to brush seals and (b) the finger pad geometry offers the potential for the pad lift off. The scope of this paper is to present for the first time, distributed models in 2-D and 3-D dimensions. We shall analyze an assembly of two fingers arranged in line. The two-dimensional model considers flow only in the axial and radial directions, Figure 2, with no leakage between adjacent fingers. The three-dimensional model considers also the flow in the circumferential direction, Figures 3 and 4. The fingers have freedom of motion in all directions. Both models incorporate fluid-structure interaction in order to account for the fingers' compliance. The 2-D approach, in fact, represents the limiting best-case scenario, when leakage occurs only through the area of the gap under the finger pad. The 3-D model represents the limiting worst-case scenario, when flow leakage moves through the pad/shaft gap and in an unrestrained mode in-between the fingers. Both 2-D and 3-D models combine in an integrated mode the Navier-Stokes equations with an elasticity

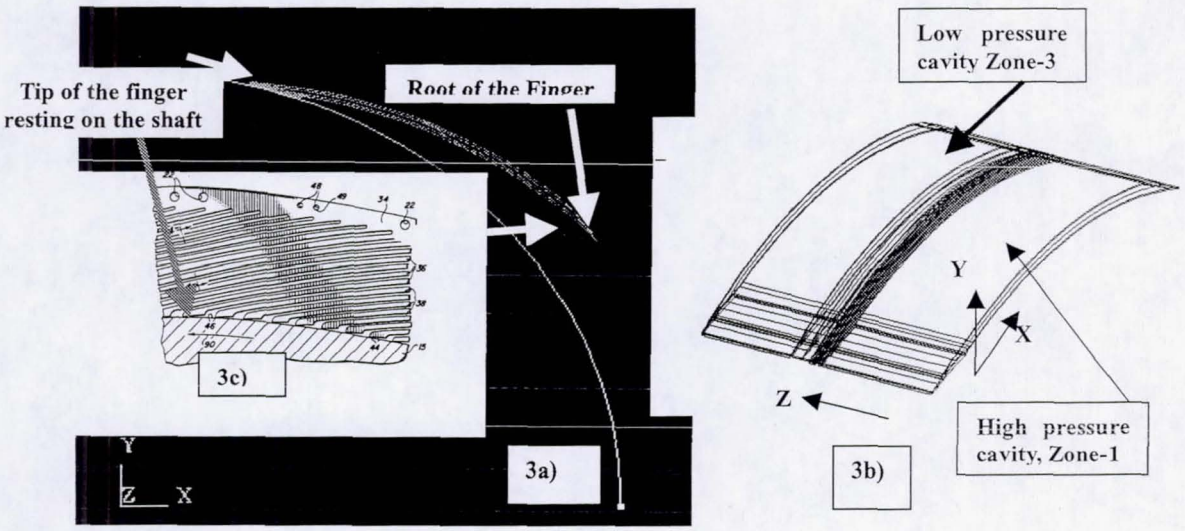

Figure 3. (3a) Typical position of one finger with its root and its pad. (3b)Arrangement of fingers in-between the cavities. Frontal view of a wafer containing pad-less fingers (Arora (1998), Patent No. 5,755.445).

model and shaft rotation, thus solving jointly for seal leakage and finger pad elastic deformation. The basic goal of this preliminary work is to establish limit cases and gain insight into the physics of flow and finger motion. Eventually this work will deliver a tool for parametric evaluation of finger seal designs that ensure both the lifting of the finger and acceptable leakages.

GEOMETRY OF THE FINGERS

We shall present here a detailed layout of the 3-D computational domain and its construction with only the mention that the grid used for the 2-D simulation was obtained through the elimination of the circumferential coordinate from the 3-D simulation. The basic geometry of the fingers

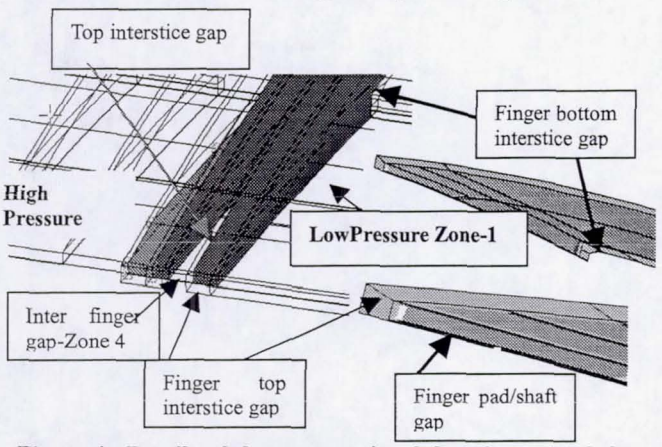

Figure 4. Details of the computational domains around the pair of in-line fingers

assembly studied here is presented in the radial-axial cross section of Figure 3 and 4. This is a modification of the Arora (1998) patent, in so far that the finger on the high-pressure side does not incorporate a pad, but rather ends at about 0.015 in above the surface of the rotating shaft. The elimination of this pad helps in the overall hydrodynamic lifting process of the pad finger off the shaft. The 3-D grid incorporating the high pressure cavity (Zone-1), the fingers, the interstice Zone-4 between the fingers, the top and bottom gaps surrounding the stick and pad and the low pressure Zone-3 is shown in Figures 3a, 3b and Figure 4. The shaft-to-pad clearance is 0.0005 in (0.0127 mm), while the elongated interstitial top and bottom gaps that separate upstream and downstream sequential fingers are 0.015 in (0.381 mm). These interstice gaps have a geometry controlled by a circumferential logarithmic curvature. While the full seal geometry has 72 fingers per row and two to three rows in the axial direction, our computational setup is limited to a pair of upstream and downstream in-line fingers (as discussed) and the gaps surrounding them. The third, axial dimension shows the cavity in front, cavity in-between and behind the two axially neighboring fingers, Figure 3b. The low-pressure finger pad if properly designed, should be able to generate sufficient hydrodynamic lifting force to offset the static pressure applied on the top of the pad by the environment. The pad thus lifted, will generate both enough pressure drop in the axial direction to act as a seal, and glide in a compliant fashion over the shaft.

Gridding.

The three-dimensional grid was obtained by extrusion of the two-dimensional X-Y grid into the third (Z) dimension, as shown by Figure 3b. This direction is aligned with the axis of the shaft. The first two-dimensional X-Y plane boundary perpendicular on the longitudinal axis was created at the position where the high-pressure cavity is starting (overall

domain inlet, Figure 3b). The two fingers and domain boundaries were projected on this plane. Grid distributions were then assigned to all of these geometric formations. The overall 3-D computational model incorporates 403,696 cells in 152 sub-domains. The grid used 60 nodes in the X-direction, 85 nodes in the Y-direction and 100 nodes in the Z-direction. Large memory requirements are due to significant amount of 3-D prismatic finite element analysis (FEA) nodes. The FEA portion of the mesh is used for the solid finger model and has to match the fluid mesh at their interface. The fluid mesh requires very small grid sizes in certain small foot print areas causing computational overhead for the FEA grid. The fluid-structure (FSI) formulation requires matching grid interfaces and the fluid cells must be structured/prismatic to allow the transfinite interpolation necessary to account for the grid movement.

NUMERICAL MODEL AND SOLUTION.

Computational Model.

The computational engine, CFD-ACE+ is a commercial software package available from CFDRC (Huntsville, Alabama). The algorithm solves the full Navier-Stokes equations in a Cartesian 2-D axisymmetric system of coordinates, and with rotating boundary conditions at the shaft surface. We utilized a conjugate gradient algebraic solver with pre-conditioning. The flow problem with no-finger deformation typically converges in 300 iterations. The flow problem with finger deformation utilizes the transient solution method. The computation used 5 iterations with very large time steps and allowed 100 sub-iterations on each time step. The algorithm utilized first order approximations for upwind terms and second order finite elements. Prismatic grids were used for both flow and solid domains. CFD-ACE+ uses absolute convergence criteria, which for pressure field usually requires convergence to 4 orders of magnitude. Convergence for finger deflections is monitored on each time step, and usually after 5 transient iterations the solution converges. The code uses an add-on module, FEMSTRESS, that interacts in a feedback mode with CFD-ACE+ to enable the calculation of stresses and deformations that develop in the finger due to the pressures and shear associated with the fluid motion. In our study we utilized FEMSTRESS's two-way transient coupling to accommodate grid motion due to the deformation of solid fingers. Solid grid deformation is calculated on each time step of the combined fluid/solid transient solution. As the finger sticks and pads deform under pressure, the flow zones (Zones 1-4, Figures 3 and 4) boundaries change shape correspondingly. Each resulting deformed shape is then used as initial geometry for the next time step. Calculations are performed until consecutive iterations converge to a final equilibrium shape. Typical computations performed on a Pentium 4 class PC with 500 Mb of RAM required a considerable amount of disk swapping. The time required to complete a typical calculation was around 15 CPU hours

Boundary Conditions.

In a typical seal operation there is high hydrostatic pressures in the front cavity of the seal (Zone-1), combined with strong rotational flow in the vicinity of the shaft (Zone-2, Figure 2). The low-pressure cavity behind the seal, Zone-3, is at atmospheric pressure. The lower boundary of the computational domain is the shaft surface and has specified rotational boundary conditions. We used linear velocities of 100m/s for the 3-D cases and 200 m/s for the 2-D cases . Outlet cavity conditions require a free-floating boundary to allow flow to develop as it may, in order to satisfy pressure and mass flow continuity conditions. For computational reasons, notwithstanding certain computational time penalty, this boundary was moved further downstream such that it would not affect the flow in the area adjacent to the second rows of fingers. Table 1 presents further characteristics of finger geometry, material and grid specifications.

For the purpose of this study we utilized velocity type boundary conditions at the inlet of Zone-1. They are easier to implement and make for a more robust computational scheme while providing a higher convergence rate. On the top and bottom sides of computational domains we also specified free-floating outlet conditions. We also have specified symmetry boundary conditions at the top and bottom boundaries of the interstices, Figure 4. Not only are these conditions possible due to the repetitive nature of the fingers and their contiguous interstices, but they are also of great benefit to the overall computational process by eliminating the need to simulate the entire circumference of the seal. Solid wall boundary conditions for the flow are applied at the stationary cavity walls and zero displacements for FEA at the finger mounting locations.

Table 1. Finger and Shaft Geometry, Material and Grid Specifications

Diameter of shaft		5.090 in (129.3 mm)
Inner diameter of the aft-finger pad		5.091 in (129.3 mm)
Initial size of the pad gap (radial)		0.0005 in (0.0127 mm)
Inner diameter of the fore-finger		5.120 in (130.048 mm)
Gap of the fore-finger (radial)		0.015 in (0.381 mm)
Pad axial width		0.100 in (2.54 mm)
Outer diameter of the finger root (stick)		5.738in (145.745 mm)
Young modulus		30E+6 psi (207 GPa)
Grid:	total number of cells	7561
	total number of structured cells	6720
	unstructured cells	841

RESULTS AND DISCUSSION

The results to be presented herein are partitioned in two sections. The first refers to two-dimensional quantitative results that investigate flow, pressures and pad deformations in the radial-axial plane. The second section examines the flow patterns around a pair of in-line fingers in a three dimensional setup.

Two-Dimensional Analysis

In this "reduced" model, all the flow passes through a 2-D axial cross section, Figure 2. NO leakage flow is allowed between the neighboring fingers in circumferential direction. Thus it represents a limiting case for the finger seal. For all practical purposes the geometry of Figure 2 is equivalent to that of continuous compliant disks around the circumference. However, the stick and pad of the finger can move both in the axial and radial directions. In this configuration the leakage flow is due only to the axial pad lift, which creates a radial gap clearance between the aft-finger pad and the runner. The fore-finger is designed with a gap of 0.015 in (0.381 mm) above the shaft, thus not being able to seal at all. In the environment of an actual finger seal with staggered fingers, the role of this fore finger is to close (seal) the top and bottom gaps between adjacent fingers on a laminate, as well as eliminate Zone-4 (Figure 2) when the high-pressure side presses the rows of fingers together. Thus, one can extrapolate and assume that a 2-D model will generate an "idealized" and lower limiting case. The two-dimensional approach considers an axi-symmetric model of rotational flow, with rotational speed specified on the shaft/runner surface. The fore- and aft-fingers deform under the pressure forces and change the clearance profile between the finger pad and the runner. That affects finger seal performance and its ability to lift and "ride" on the film surface. The Zone-1 inlet velocity boundary condition has been set to 1.64 ft/s (0.5 m/s) and the shaft is rotating at 656 ft/s (200m/s).

Figure 5a (inset) presents the total velocity contours, and superimposed on them the axial velocities as the flow progresses through the gap. One must note that even though inlet velocity boundary condition is very low, the maximum velocity in the gap reached 938.32 ft/s (286 m/s). The corresponding pressure drop is approximately 54.7 psi (377 kPa) and the mass flow rate 7.1E-4 lbm/s (3.22E-4 kg/s) . The pressure drop in the gap is shown in Figure 5b, where for the reader orientation we have superimposed below the length of the gap containing the velocity contours. Note that each dot on the pressure curve corresponds to a dot on the abscissa of the superimposed gap. One can notice that the pressure in the high-pressure cavity does not drop at all as the flow enters the recessed (0.015in (0.381 mm) pad-less fore-finger and crosses the interstice between the two fingers. However, the entrance under the aft-finger gap engenders a quick and steep pressure drop. As it appears from the further study of Figure 5b, the

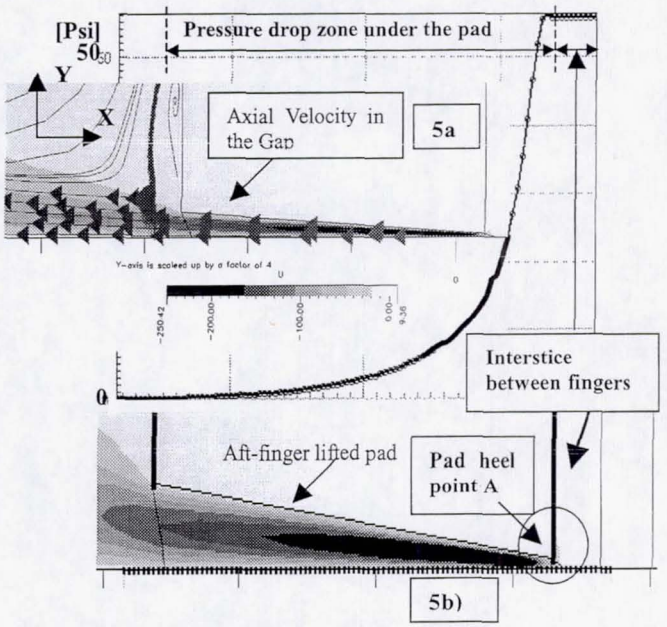

Figure 5. (5a) Axial velocity profiles in the gap. (5b) Pressure profiles under the pad and associated velocity contour profiles

pressure under the pad becomes close to the low cavity pressure a little bit ahead of the trailing edge of the pad, indicating that possibly the pad can be shortened. Since the pad was positioned with a very small gap above the shaft, the axial flow under it is completely pressure induced and the pressure generated both lifts and rotates the pad with respect to its heel point A (x=y=0). The effects of rotation are accounted in the framework of an additional equation for rotational velocity in the axi-symmetric coordinates.

For the operational conditions with finger elastic deformation, pressure drops across the pad decrease from 54.7 psi (377kPa) with shaft rotation, to 13 psi (90kPa) without rotation. In the case of the non-deforming finger pressure drop decreases from 84 psi (580kPa) with shaft rotation to 72 psi (500kPa) without rotation. Figures 6a and 6b present the deformation of the pad under static pressure effects. The static pressure acting in, Zone-1, causes an axial displacement and deformation of both the stick and the pad as shown in Figure 6a. Note the significant axial deformation of 0.004 in (-1.1 E-4 m). Figure 6b, presents the radial lifting and deformation of the stick-pad assembly. A study of the scale bar reveals that the heel A is actually deflected downward toward the runner, causing a sort of a pinch point and reducing further the seal clearance. The trailing end of the pad deflects upward by approximately 0.0017 in (4.2E-5 m). It is worth noting that the fore-finger stick deformations and motion, either radially or axially, is negligible since the axial momentum imparted by the flow (running at 1.64 ft/s (0.5 m/s)) is very low.

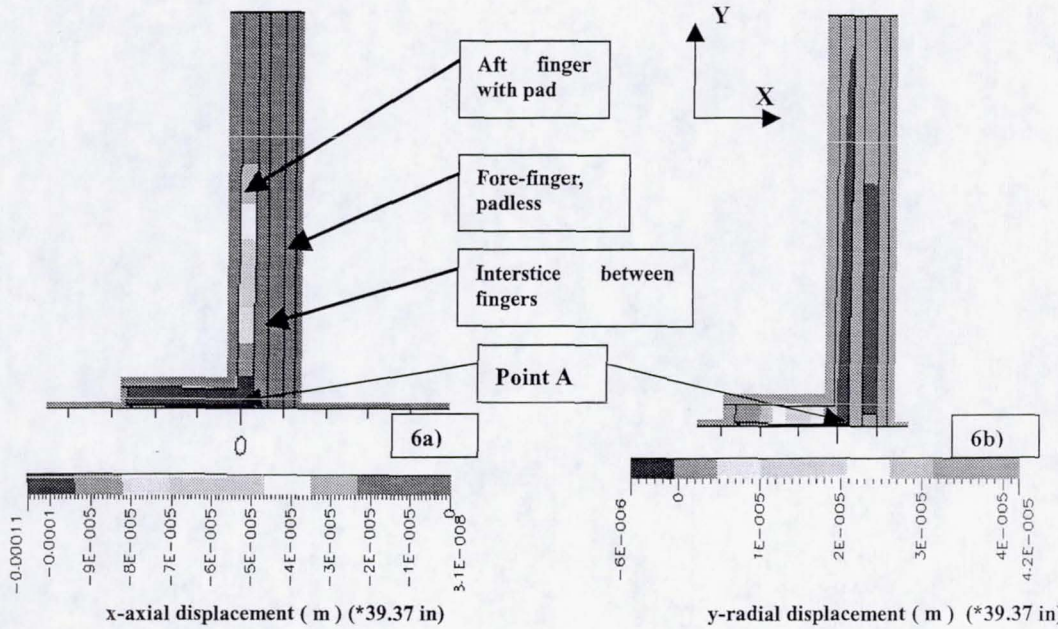

Figure 6.Axial and radial displacements of the pad.

Three-Dimensional Analysis

Three specific cases were studied. In all cases the pair of fingers is arranged in-line and the flow moves unrestrained around the fingers through the in-line interstices. Such a situation is equivalent to the case when the axially staggered finger laminates of a finger seal, Figures 1b and 2, do not seal the interstices between the adjacent fingers distributed in the circumferential direction.

High Axial-Velocity Case (V_{axial}= 328ft/s (100 m/s)). *Figure 7 presents the numerical simulation of the flow across a* pair of fingers like the ones shown schematically in Figure 2. The high-pressure finger is pad-less while the low pressure one contains a pad as shown in the figure. The three dimensional rendition can be revisited in Figure 4. The fingers separate the high-pressure Zone–1 from the low pressure Zone-3. As already mentioned, the upstream boundary conditions are velocity driven. The study of the figure indicates that the main path for flow leakage is through the bottom and top interstices, which represent gaps between sequential fingers. One can clearly see (as marked) particle tracers trajectories flowing through the top gap and bottom respectively. The axial flow effect is that strong in Zone 1 in the vicinity of the fingers, that no flow trajectories are visible in the circumferential direction. However, in Zone-3 as the computation moves away from the finger area, there seem to appear circumferentially oriented flow patterns. That can be attributed to the decrease in the axial momentum of the flow as it passes through the top and bottom gaps.

Medium Axial-Velocity Case (V_{axial}=164 ft/s (50 m/s)). Figures 8a and 8b present an intermediate case where the axial velocity has been decreased by a factor of two. Figure 10a presents the flow in Zone-1 in the vicinity of the pair of fingers. It can be seen that while far upstream the axial effects are undeterred, as the flow moves closer to the fingers, due to the necessary change in direction, the axial momentum diminishes considerably, and in the region of the pads the flow starts a strong circumferential motion. Figure 8b presents the flow both in the low pressure Zone-2, and in the interstice Zone-4 between the fingers. In both zones the circumferential momentum is just starting to dominate, forcing the flow to strongly change direction and follow the motion of the shaft. However one can also see clearly that the axial flow still plays a significant role. Apparition of the circumferential flow is a sign that the sealing effects are increasing, since such circumferential flow acts itself as a barrier to leakage.

Low Axial-Velocity Case (V_{axial}= 3.28 ft/s (1 m/s). Figure 9 presents the flow around the two in-line fingers when the velocity boundary condition at the inlet of Zone-1 has been decreased by a factor of 100 from the high speed original case presented. One can observe that the flow is now predominantly oriented in the circumferential direction in all three zones shown (1, 4 and 3). The detail in Figure 9a also shows in three-dimensional format predominantly the flow in the in-between finger interstice as well as the region immediately adjacent to the high-pressure finger of Zone-1.

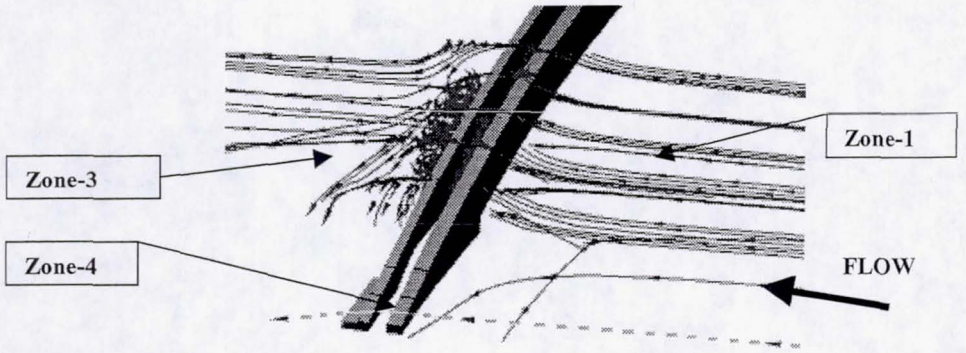

Figure 7. Flow/leakage between high pressure Zone 1 and low pressure Zone 3 when the shaft interface velocity is 100m/s and the inlet axial velocity of flow to Zone-1 is 100m/s

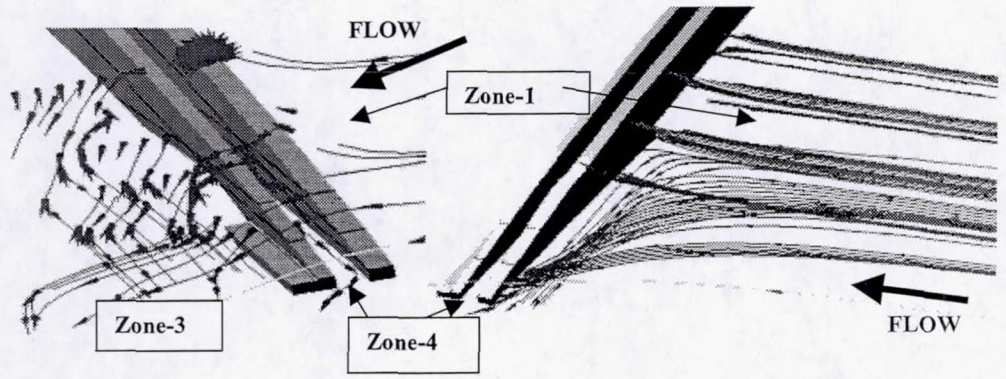

Figure 8. Flow/leakage between high pressure Zone 1 and low pressure Zone 3 when the shaft interface velocity is 100m/s and the inlet axial velocity of flow to Zone-1 is 50m/s

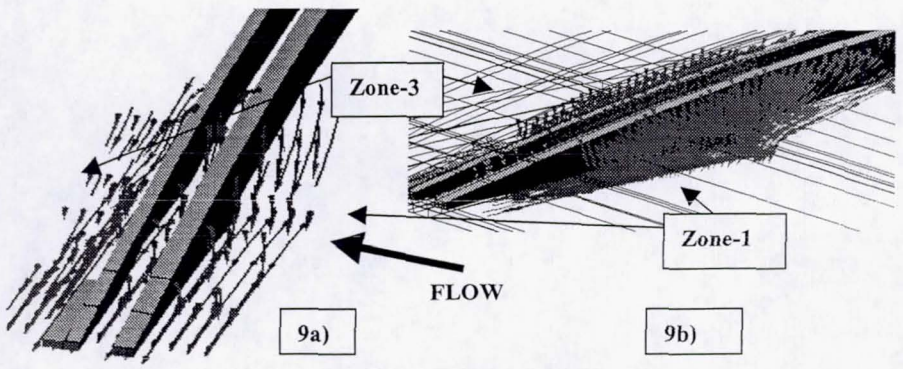

Figure 9. Flow/leakage between high pressure Zone-1 and low pressure Zone-3 when the shaft interface velocity is 100m/s and the inlet axial velocity of flow to zone-1 is 1 m/s

CONCLUSIONS

The two- and three-dimensional numerical experiments considered here represent two limiting cases for the behavior of a finger seal. Thus, the 2-D case is equivalent to a finger seal where there is no flow through interstices between the fingers, while the 3-D cases present the worst case scenario, i.e. when the interstices between sequential fingers act as in-line sequential orifices with practically no capability for sealing. The results of Figure 5 and 6 show that the finger pad will have a deformation with rotation in the axial direction, thus becoming misaligned longitudinally with respect to the shaft. This imposes the necessity to design the pads for minimum axial deformation and rotation. For the geometry of the pad studied here it was found that in the 3-D case the radial motion of the pad upward was only minute. The 3-D studies of the flow show that the velocity and geometry of the flow in Zone-1 (high pressure) influences decisively the flow in the vicinity of the fingers. Thus, high axial velocity flows easily penetrate the zones in-between sequential fingers, while low axial velocities allow rotational effects in the vicinity of the fingers to take over. As well, it is clear that width of the interstices between the fingers needs to be as small as possible in order to minimize leakage through the body of the FS. Finally the study presented here provides insights into the physics of the compliant fingers and, in the authors' opinion, represents a first step towards the simulation of the finger seal staggered geometry.

ACKNOWLEDGEMENTS

The authors want to express their gratitude to Mr. Robert C. Hendricks of NASA Glenn Research Center, Cleveland, Ohio, for his many timely comments and suggestions during the performance of the work described in this paper.

REFERENCES

Arora, G.K., 1998, "Noncontacting Finger Seal with Hydrodynamic Foot Portion", Patent No. 5,755,445

Arora, G.K., Proctor, M.P., Steinetz, B.M., "Pressure Balanced, Low Hysteresis Finger Seal Test Results", NASA TM 1999-209191.

Atkinson, E. and Bristol, B., 1992. Effects of Material Choices on Brush Seal Performance, *Lubrication Eng., Vol. 48, pp 740-746.*

Braun, M.J, Hendricks, R.C., Canacci, V., 1990. Non-Intrusive Qualitative and Quantitative Flow Characterization and Bulk Flow Model for Brush Seals, *Proceedings of the Japan Int. Tribology Conference, Vol. III, pp. 1611-1616,* Nagoya, Japan.

Chupp, R.E., Dowler, C.A., 1991. Performance Characteristics of Brush Seals for Limited Life Engines, *36th ASME Gas Turbine Conference, Orlando,* Florida, paper no. 91-GT-281.

Chupp, R.E., Holle, G.F., "Simple Leakage Flow Model for Brush Seals", the *AIAA/SAE/ASME 27th Joint Propulsion Conference*, Sacramento, California, June 1991.

Chupp, R.E., Holle, G.F., "Generalizing Circular Brush Seal Leakage Through a Randomly Distributed Bristle Bed", Presented at the *International Gas Turbine and Aeroengine Congress and Exposition*, The Hague, Netherlands, June 1994.

Fergusson, J.G., 1988, "Brushes as High Performance Gas Turbine Seals", Paper Nr. 88-GT-182, ASME Gas Turbine and Aero Engine Congress, Amsterdam, The Netherlands, June 6-9.

Forry, J.M., 1993. High Temperature Brush Seals and High Pressure Ratio Swept Fan Program, *High Temperature Brush Seals, Vol. 1, Wright Labs. Technical Report no. WL-TR-94-2007*

Hendricks, R. C., Schlumberger, S., Braun, M. J., Choy, F. K., and Mullen, R., 1991, "A Bulk Flow Model of a Brush Seal System", Paper presented in the 36th *ASME Int. Gas Turbine Conference, Orlando, Florida, June.*

Hendricks, R.C., Griffen, T.A., Bobula, G.A., Bill, R.C., Howe, H.W., 1992. Integrity Testing of Brush Seal in a T-700 Engine, *NASA Conference Publication 10124, NASA Lewis Research Center Seals Workshop,* Cleveland, Ohio, pp. 117-138.

Hendricks, R.C., O'Halloran, B., Arora, G., Addy, H.E., Flowers, J., Carlile, J., Steinetz, B.M., "Advances in Contact Sealing", NASA CP 3282, Vol. 1, pp 363-371.

Heydrich (1991), Bi-directional Finger Seal, Patent 5,031,922

Johnson, M.C., 1992, Laminated Finger Seal with Logarithmic Curvature, US Patent 5,108,116

Lattime, S.B., 2001, "A Hybrid Floating Brush Seal (HFBS) For Improved Sealing And Wear Performance In Turbomachinery Applications", Ph.D. Thesis, University Of Akron, Dept. of Mechanical Engineering

Ludwig, L., 1978, "Self-Acting Shaft Seals", Seal Technology in Gas Turbine Engines, *AGARD Conference Proc. No. 237*

Mackay, C.G., 1991, Laminated Finger Seal, Patent 5,042,823

Mackay, C.G., 1991a, Laminated Finger Seal, Patent 5,071,138

Mullen, R.L., Braun, M.J., Hendricks, R.C., 1990, "Numerical Modeling of Flows in Simulated Brush Seal Configuration" Paper #90-2141, *AIAA/SAE/ASME/ASEE 26th Joint Propulsion Conference*, July 16-18, Orlando, Florida,,

Proctor, M.P., Walker, J.F., Perkins, H.D., Hoopes, J.F., and Williamson, G.S., 1996. Brush Seals for Cryogenic Applications: Performance, Stage Effects, and Preliminary Wear Results in LN_2 and LH_2, *NASA Technical Paper no. 3536.*

Steinetz, B.M., Hendricks, R.C., Munson, J., "Advanced Seal Technology Role in Meeting Next Generation Turbine Engine Goals", NASA –TM 1998-206961, 11 pages